B. pertussis tracheal cytotoxin biases NOD signaling to suppress IL-1 mediated inflammation and evade adaptive immunity

David M. Rickert[1], Elizabeth Hill[1], Riley Himmelberger[1], Neeta Rajbanshi[1], Sasha Cardozo[1], Tialfi Bergamin de Castro[2], Ravi Bharadwaj[3], Alison J. Scott[1,2], Neal Silverman[3], William E. Goldman[4], Nicholas H. Carbonetti[1], Karen Scanlon[1], Ciaran Skerry[1]

Affiliations
[1]Department of Microbiology and Immunology, University of Maryland School of Medicine, Baltimore, MD, USA
[2]Department of Microbial Pathogenesis, University of Maryland School of Medicine, Baltimore, MD, USA
[3]Program in Innate Immunity and Division of Infectious Diseases and Immunology, Department of Medicine, University of Massachusetts Chan Medical School, Worcester, MA, USA
[4]Department of Microbiology, University of North Carolina School of Medicine, Chapel Hill, NC, USA

Graphical abstract

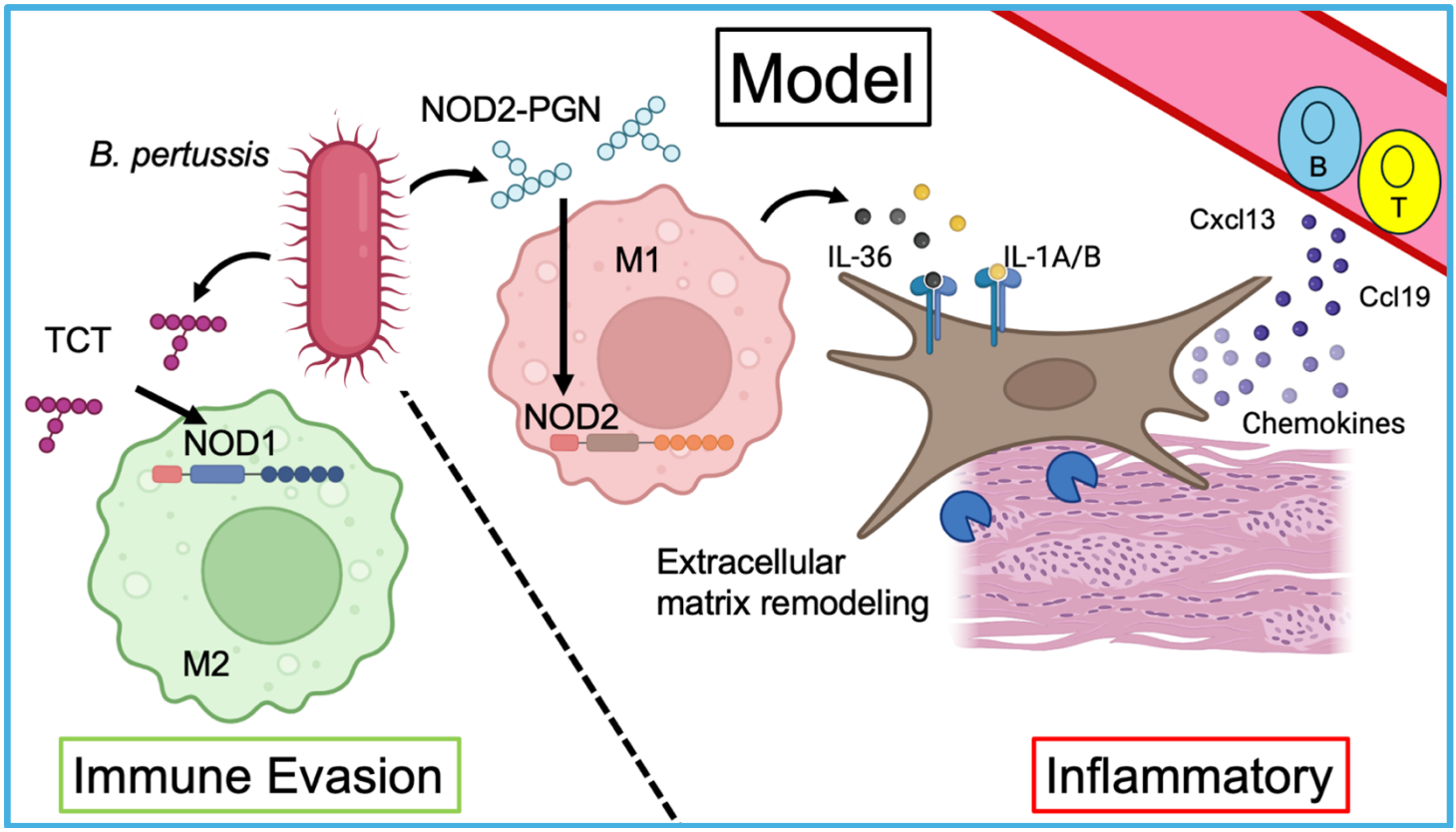

Highlights

- *B. pertussis* produces both NOD1 and NOD2 activating PGNs.
- Release of TCT polarizes toward NOD1 responses.
- NOD2 activation in myeloid cells drives IL-1 family cytokine production.
- IL-1 family cytokines skew fibroblasts towards an inflammatory phenotype, leading to chemokine release, extracellular remodeling, and recruitment of lymphocytes
- TCT release dampens the recruitment of adaptive lymphocytes to facilitate bacterial persistence.

ABSTRACT

Bordetella pertussis, the causative agent of whooping cough, is a Gram-negative bacterium, which colonizes the respiratory tract and evades clearance through multiple virulence factors. One such factor, tracheal cytotoxin (TCT), is a monomeric peptidoglycan (PGN) fragment released extracellularly due to inefficient recycling by the permease AmpG. Although TCT is known to be a potent NOD1 agonist *in vitro*, its role *in vivo* remains poorly defined. Here, we demonstrate that TCT release during infection suppresses pulmonary inflammation. Mice infected with a TCT over-releasing strain, TCT(+), exhibited reduced lung immunopathology compared to wild-type or TCT-under releasing, TCT(-), strains. Reporter assays revealed that TCT(+) preferentially enhanced NOD1 activation, while TCT(-) strains skewed signaling towards NOD2. *In vivo,* NOD2 knockout mice displayed reduced lung inflammation, implicating NOD2-driven responses in pulmonary pathology. Transcriptomic analysis identified IL-1β as closely associated with expression of NOD2 but not NOD1. In support, TCT(+) infection led to reduced IL-1β protein levels than WT or TCT(-). CellChat analysis of single-cell RNA-sequencing data identified alveolar macrophages as the primary source of IL-1β and airway fibroblasts as key responders. Infected airway fibroblasts upregulated inflammatory chemokines such as CXCL13 and CCL19, promoting lymphocyte recruitment. Proteomic profiling and flow cytometry confirmed reduced chemokine levels and B cell recruitment in TCT(+) infections. Importantly, IL-1 receptor knockout mice showed significantly impaired recruitment of B and CD4+ T cells and higher bacterial burdens, despite unchanged innate cell infiltration. This underscores the role of IL-1 in coordinating adaptive immunity. Together, these findings support a model in which TCT release skews host signaling towards NOD1, suppresses NOD2 and IL-1 mediated fibroblast activation, blunts chemokine-driven lymphocyte recruitment, and impairs adaptive immune clearance. These results suggest that TCT release is an immune evasion strategy to dampen inflammation, prolong persistence and prevent the development of protective adaptive responses and highlights divergent outcomes following engagement of NOD1 or NOD2 during infection.

INTRODUCTION

Bacterial pathogens have evolved diverse mechanisms to manipulate the host response in to promote their survival and persistence. Many pathogens strategically alter the structure or availability of pathogen-associated molecular patterns (PAMPs) to shape the host immune responses. For example, many Gram-negative bacterial pathogens modify the structure of the lipid A region of lipopolysaccharide (LPS) to control the magnitude of the host immune responses[1]. However, the impact of peptidoglycan (PGN) structure on host responses to bacterial infections has been less studied.

Peptidoglycan, a conserved component of the bacterial cell wall, forms a mesh-like polymer of repeating disaccharides crosslinked by short peptides[2]. The host immune system recognizes conserved PAMPs like PGN to initiate inflammatory responses. Cytosolic receptors NOD1 and NOD2 detect PGN motifs; such as Diaminopimelic acid (DAP) and muramyl dipeptide (MDP) or NagK phosphorylated MDP, triggering NF-kB-mediated inflammatory signaling[3-5]. This places selective pressure on bacterial pathogens to modify muropeptide release or the biochemical structure to evade immune responses.

Interestingly, several unrelated bacterial pathogens have independently evolved the ability to actively release specific muropeptides during infection. *Borrelia burgdorferi*, *Neisseria gonorrhea* and *Bordetella*

pertussis release free PGN fragments, an energetically costly process, which could increase immune detection[6,7]. *Both N. gonorrhea* and *B. pertussis* preferentially release a GlcNAc(beta1-4)-MurNAc(1,6-anhydro) DAP-type tetrapeptide, termed TCT in *B. pertussis*[8,9].

Prior studies have demonstrated that TCT promotes extrusion of ciliated cells *in vitro*, thereby impairing mucociliary clearance of the pathogen[10]. Additional *in vitro* studies have linked TCT to pro-inflammatory signaling, including enhanced iNOS and IL-6 production and break down of barrier integrity[11]. However, TCT's *in vivo* effects remain largely unexplored. To address this gap, we investigated the role of TCT during *B. pertussis* infection and immunopathology. We employed *B. pertussis* strains engineered to overproduce or limit TCT to assess its role *in vivo*. The permease AmpG recycles anhydro-muropeptides from the periplasm into the cytoplasm for reuse[12]. *B. pertussis* expresses an inefficient AmpG, resulting in periplasmic accumulation and extracellular release of TCT[6,13]. Replacing the native *ampG* with the more efficient *E. coli* version reduced TCT release by ~98% (TCT(-)) without affecting bacterial growth[14]. Conversely, deletion of the native *B. pertussis ampG* resulted in a 24-fold increase in TCT release without compromising growth, producing a TCT-over-releasing strain (TCT(+))[15].

To evaluate the *in vivo* impact of TCT release, we challenged mice with TCT(+), TCT(-) or wild-type (WT) strains of *B. pertussis*. Contrary to prior *in vitro* studies linking TCT to inflammation, we observed an unexpected anti-inflammatory effect of TCT *in vivo*. Reporter assays and single cell transcriptomics revealed that TCT selectively engages NOD1 over NOD2 contributing to its anti-inflammatory effects. We identify a NOD2-IL1 signaling axis in which IL-1 activates IL1R1+ airway fibroblasts to promote inflammatory extracellular matrix remodeling and chemokine production. Our data suggests *B. pertussis* exploits selective TCT release to bias host sensing of PGN towards NOD1, thereby avoiding pro-inflammatory NOD2 activation. This TCT-mediated immune skewing impairs adaptive immune recruitment, facilitating bacterial persistence in the respiratory tract and preventing the seeding of effective immune memory responses. Further, it highlights divergent outcomes of PGN signaling via NOD1 or NOD2 during infection. These findings have broad implications for understanding bacterial immune evasion, PGN sensing, vaccine adjuvant development, and the design of live attenuated vaccines such as BPZE1, which has been engineered to limit TCT release[14].

RESULTS

TCT dampens pulmonary inflammation in vivo

To investigate the contribution of tracheal cytotoxin (TCT) to the pathogenesis of *Bordetella pertussis* infection *in vivo*, we intranasally challenged mice with wild-type (WT), TCT-over-releasing (TCT(+)), or TCT-under-releasing (TCT(-)) strains of *B. pertussis*. Based on prior *in vitro* studies describing TCT as a pro-inflammatory PAMP, we hypothesized that infection with the TCT(+) strain would induce heightened pulmonary inflammation. Surprisingly, we observed the opposite outcome: mice infected with the TCT(+) strain exhibited significantly reduced lung inflammation compared to those infected with the WT strain (Figure 1A–D). Histological analysis of lungs at 7 days post-infection (dpi) revealed diminished immune cell infiltration and less bronchovascular bundle cuffing in the TCT(+) group than WT or TCT(-) (Figure 1A–C).

To determine whether differences in immunopathology were due to discrepancies in bacterial load, we quantified lung colony-forming units (CFUs) at 2 and 7-dpi. No significant differences in CFU were observed between strains at either time point (Figure 1E), indicating that inflammation was not driven by discrepancies in bacterial burden. We also assessed *in vitro* growth of the WT, TCT(-), and TCT(+) strains in Stainer-Scholte medium and found no differences in doubling time, further suggesting differences in pathology were not due to fitness defects in the mutant strains (Sup. Figure 1A, B).

To determine whether innate immune cell recruitment contributed to the observed differences in pulmonary immunopathology, we next characterized infiltrating immune cells in the lung. Consistent with histology data showing reduced immunopathology, TCT(+) challenge resulted in significantly reduced recruitment of neutrophils, macrophages and inflammatory monocytes, but no significant differences in dendritic cells in the lung at 7-dpi (Figure 1F-I). These results demonstrate that TCT release directly limits pulmonary immune cell recruitment and inflammatory pathology. To further assess how TCT influences the dynamics of immune cell recruitment, we analyzed inflammatory cell populations in the lungs at 4-dpi. No significant differences in the total number of neutrophils, macrophages, inflammatory monocytes or dendritic cells were noted between groups at this time-point (Sup. Figure 1C-F). However, TCT(+)-infected mice exhibited a shift in macrophage polarization, with an increased frequency of M2 macrophages and a decrease

in M1 macrophages relative to WT and TCT(-) challenge (Figure 1J, K). This shift is consistent with a more pro-resolving immune profile in TCT(+) challenged mice, as M2 macrophages are typically associated with anti-inflammatory and tissue repair functions unlike pro-inflammatory M1 macrophages[16].

These findings suggest that TCT release alters the inflammatory signaling milieu early during infection in the lung leading the divergent pulmonary inflammation observed at 7-dpi. To further assess this, we performed bulk RNA sequencing of 4-dpi lungs from mice infected with WT, TCT(-), or TCT(+) strains. Consistent with earlier histopathology data, mice infected with the TCT(-) strain exhibited a pronounced upregulation of pro-inflammatory transcripts, whereas TCT(+)-infected mice showed a transcriptional profile indicative of dampened inflammation compared to WT (Figure 1L, M). Notably, TCT(-) infection induced higher expression of inflammatory cytokines and chemokines such al *Il1b, Il6, Il21, Il1b, Il6, Il21, Il22, Il23a, Il33, Il36g, Ccl3, Ccl19*, *Cxcl5*, and *Cxcl13* (Figure 1N). Conversely, TCT(+) infection led to reduced expression of *Il1a, Il2b, Ccl2, Cxcl9, Cxcl10* and *Cxcl11* relative to WT infection (Figure 1O). Importantly, *il1b* and *nos2*, two transcripts associated with M1 macrophage polarization, were significantly upregulated in TCT(-) infected lungs, reinforcing the link between TCT release and the inhibition of M1 polarization (Figure 1L). These data suggest that TCT release promotes an anti-inflammatory state by skewing macrophage polarization toward M2 phenotypes and suppressing key pro-inflammatory pathways. Contrary to earlier *in vitro* studies, our findings demonstrate that TCT acts as a suppressor of inflammation *in vivo* during *B. pertussis* infection.

Increased release of TCT decreases NOD2 activation

To investigate the mechanism by which TCT dampens *B. pertussis*-induced lung inflammation, we first evaluated the signaling activity of purified TCT in mouse and human NOD1 and NOD2 reporter cell lines. Consistent with prior reports, TCT selectively activated murine and human NOD1 but failed to stimulate NOD2 signaling (Sup. Figure 2A-D)[17,18]. TCT potently activated murine NOD1 signaling, with measurable responses above control observed at concentrations as low as 100 pg/mL (Sup. Figure 2A). While TCT activated human NOD1, the response was less sensitive than that observed in murine NOD1 (Sup. Figure 2B). Prior studies suggest that this difference may be due to lower expression of muropeptide transporter SLC46A2 in human reporter cells; overexpression of SLC46A2 in human NOD1 reporter lines has been shown to enhance sensitivity to TCT[17]. Notably, human reporter cells expressing murine NOD1 do not require enhanced SLC46A2 expression for robust responsiveness, suggesting murine NOD1 recognizes TCT with significantly greater potency (Sup. Figure 2A, B). We assessed TCT's ability to stimulate murine and human NOD2 via reporter cell assays and confirmed both murine and human NOD2 are not activated by TCT, confirming TCT strictly activates NOD1 and not NOD2 (Sup. Figure 2C, D)[18].

To determine whether differences in TCT release among *B. pertussis* strains influence NOD1 and NOD2 activation, we co-incubated wild-type WT, TCT(-) and TCT(+) strains with murine NOD1 and NOD2 reporter cells. As expected, the TCT(-) strain elicited the weakest NOD1 response, while the TCT(+) strain induced the strongest (Figure 2A). Interestingly, the opposite pattern was observed for NOD2 signaling; the TCT(-) strain induced the greatest NOD2 activation, whereas the TCT(+) strain induced the lowest (Figure 2C). WT and TCT(-) *B. pertussis* induced significantly greater NOD2 activation than TCT(+). These data indicate that *B. pertussis* PGNs are capable of activating NOD2 and that TCT release inversely correlates with this activity (Figure 2A, C). This could potentially be due to masking or competitively inhibiting access to NOD2-stimulatory muropeptides.

To confirm that the NOD activation profile observed was due to secreted bacterial products, such as TCT, we evaluated the NOD activating profiles of conditioned media collected from these strains. These experiments mirrored the findings from whole-cell co-incubations. Conditioned media from the TCT(+) strain induced stronger NOD1 but weaker NOD2 activation, while media from the TCT(-) strain elicited stronger NOD2 but weaker NOD1 activation (Figure 2B, D). These data support the conclusion that TCT is the dominant NOD1 agonist in the media, suggesting that high levels of TCT might interfere with the release, accessibility or host-recognition of distinct NOD2-stimulatory PGN fragments. Additionally, TCT could function as a molecular decoy, competitively inhibiting the recognition of cell wall associated PGN by the host. We hypothesize that the increased NOD2 signaling observed in TCT(-) infection results from the unmasking or accumulation of a distinct, unidentified NOD2 agonist that is otherwise retained or masked in the presence of abundant TCT.

Opposing Outcomes of NOD1 and NOD2 Signaling Shape Host Inflammatory Responses to *B. pertussis*

To determine if NOD polarization could contribute to TCT-induced reductions in immunopathology we infected wild-type (WT), NOD1 (NOD1 KO) and NOD2 deficient (NOD2 KO) mice with *B. pertussis* and assessed the lung inflammatory pathology at 7-dpi. Significantly reduced bronchovascular bundle formation and alveolar consolidation was noted in NOD2 KO compared to WT mice (Figure 2E, G, I), suggesting NOD2 is a driver of host inflammation and immunopathology following *B. pertussis* infection. In contrast, NOD1 KO mice exhibited similar levels of inflammation relative to WT controls, though any potential increased inflammation in NOD1 KO mice may have been masked by the already substantial pathology observed in WT mice (Figure 2E, F, I).

To determine if the observed differences in inflammation were due to altered bacterial burden, we measured pulmonary CFU across the infection time-course. No differences in bacterial load were observed between WT, NOD1 KO and NOD2 KO mice (Figure 2H), indicating that the reduced inflammation in NOD2 KO mice was not due to differences in bacterial burden. To assess differences in NOD1 and NOD2 driven immune cell infiltration we performed flow cytometry from these same groups. NOD1 KO mice exhibited no significant difference in number of neutrophils (CD11b+Ly6g+) and macrophages (CD11b+CD14+), inflammatory monocytes (Ly6cHI, Class II HI) or dendritic cells (CD11c+CD14-), compared to WT controls (Figure 2J-M), consistent with histopathology data (Figure 2I). Strikingly, decreased numbers of neutrophils and inflammatory monocytes were observed in the lungs of the infected NOD2 KO mice compared to WT mice (Figure 2J-L), highlighting NOD2 as a critical driver of neutrophil and monocyte recruitment and suggesting these cells may be key contributors to the differences in pathology observed between WT and NOD2 KO mice. Similarly to NOD1 KO mice, NOD2 mice exhibited no differences in macrophage and dendritic cell recruitment, compared to WT controls (Figure 2K, M).

To determine if NOD1 and NOD2 contribute to observed differences in macrophage polarization (Figure 1J, K), we analyzed M1 and M2 macrophage subsets in the lungs of infected mice. While NOD2 KO mice showed no difference from WT controls, NOD1 KO mice displayed a significant increase in percent of M1-skewed macrophages (%CD86+ CD45+CD11b+CD14+) (Figure 2N). These data implicate NOD1 in suppressing M1 polarization during infection. Furthermore, we observed a non-significant ($p=0.09$) decrease in M2 polarized macrophages (%CD206+CD45+CD11b+CD14+) in the infected NOD1 KO compared to WT controls (Figure 2O). Since IL-1β production is a classical hallmark of M1 macrophage activation, we measured *il1b* transcript levels in infected lungs. NOD1 KO mice showed a ~60-fold increase compared to WT (Figure 2P), further supporting a role for NOD1 in limiting IL-1-mediated inflammation. These findings are consistent with reports from other inflammatory models in which NOD1 deficiency similarly exacerbated inflammation[19-21]. Because NOD1 and NOD2 are intracellular receptors, bacterial muropeptides such as TCT must be transported into the cytosol to be sensed. Previous studies identified SLC46A2 as a transporter for TCT and critical for skin models of inflammation [17,21]. To evaluate whether SLC46A2 contributes to TCT's anti-inflammatory effect, we infected WT and SLC46A2 KO mice and compared pulmonary bacterial burden and histopathology. We observed no differences between genotypes in either CFU or lung inflammation (Sup. Figure 3C, D), suggesting that SLC46A2 is not essential for TCT's *in vivo* function in this context. Supporting this, single-cell RNA sequencing data revealed minimal SLC46A2 expression across all pulmonary cell types at 4-dpi (Sup. Figure 3A, B).

TCT suppresses IL-1 production by biasing NOD signaling in alveolar macrophages

We have identified divergent outcomes of NOD1 and NOD2 signaling during *B. pertussis* infection (Figure 2). To gain insight into the mechanism driving these differences in inflammatory outcomes between NOD1 and NOD2 KO mice, we performed single cell RNA sequencing on lungs from sham PBS-treated control and 4-dpi mouse lungs (Figure 3A, B). We used cell-type prediction algorithms to profile the cellular landscape during *B. pertussis* infection compared to the PBS sham challenged control (Figure 3A, C). Mapping NOD receptor expression across cell types revealed that NOD1 was broadly expressed across nearly all lung cell types, while NOD2 expression was more restricted, confined primarily to subsets of neutrophils, alveolar macrophages (AMs), and inflammatory monocytes (iMONs), as well as a subset of dendritic cells (cDC2s) (Figure 3D, E).

We have demonstrated TCT mediated skewing of AM polarization (Figure 1L). To investigate functional differences in these populations we performed subcluster analysis on AM populations in our single cell RNA sequencing dataset. We identified five transcriptionally distinct clusters of AMs, dubbed clusters 0-4 (Figure 3F). Two clusters (clusters 1 and 2) appeared to demonstrate significant upregulation of pro-inflammatory

genes (Figure 3G). We identified key markers for these clusters, and discovered cluster 1 was characterized by high expression *Ly6c2, Aoah, Nos2, Fmnl2, and Slamf7*, while cluster 2 was characterized by moderate expression of those genes in addition to high expression of *Msr1, Lrg1, Wfdc17, Ccl9, and Cxcl3* (Figure 3G). Nos2 has previously been linked to the effects of TCT in vitro, suggesting peptidoglycan-mediated responses could be driving the divergent AM cluster phenotypes[11]. We performed KEGG pathway analysis on each clusters' differentially expressed genes to identify which pathways were upregulated in each AM cluster. Excitingly, NOD-like receptor signaling pathways was identified as the top enriched pathway in both clusters 1 and 2, further highlighting the importance of NOD1 and NOD2 in shaping responses to *B. pertussis* infection (Sup. Figure 4A, B). We assessed NOD1 and NOD2 expression across these AM clusters and discovered that while NOD1 was ubiquitously expressed across each of the clusters, NOD2 expression was restricted primarily to clusters 1 and 2 (Figure 3H).

To delineate the roles of NOD1 and NOD2 in our single cell dataset, we stratified AMs based on NOD1+NOD2- and NOD1-NOD2+ expression profiles and performed differential gene expression analysis, excluding double-positive cells to isolate pathway-specific effects (Figure 3K). Distinct gene expression patterns emerged. Notably, NOD2+ AMs showed strong enrichment for *il1β* and *il1α* (Figure 3L). This link between NOD2 and IL-1 family cytokines was not observed in NOD1+ cells (Figure 3L). We assessed IL-1α, and IL-1β expression in our subclusters of AMs and found that expression of these IL-1 cytokines was heavily enriched in clusters 1 and 2, overlapping with expression of NOD2 but not NOD1 (Figure 3H). Furthermore, genes associated with pro-inflammatory clusters 1 and 2, e.g., *Aoah*, were found to be associated with NOD2 expression (Figure 3L). This further implicates NOD2, but not NOD1, as a driver of the pro-inflammatory program in AMs during *B. pertussis* infection (Figure 3L). GO pathway enrichment analysis on genes identified as NOD2 associated identified positive innate immune pathways, while NOD1 associated genes were enriched in homoeostatic pathways and fatty acid metabolism, suggesting a possible link between NOD1 and immunometabolism (Sup. Figure 4C, D). Surprisingly, while IL-1α and IL-1β were strongly associated with NOD2-expressing AMs, IL-18, another IL-1 signaling cytokine, was associated with NOD1-expressing cells (Figure 3L).

To determine if TCT drives polarization of NOD1 and NOD2 responses and subsequent immune outcomes, we investigated bulk-transcriptomic data comparing WT, TCT(+) and TCT(-) infected mouse lungs and performed Ingenuity Pathway Analysis (IPA) to predict upstream regulators driving differential gene expression. IPA identified IL-1β as the top predicted upstream regulator of differences between WT and TCT(-) infected mice (Figure 3I). This further suggests that TCT dampens IL1 driven inflammation. Similarly, *Il1a* and *Nod2* were among the top upstream regulators distinguishing the inflammatory signatures of WT and TCT(+) infected mice, implicating the NOD2-IL-1 axis as a key driver of *B. pertussis* lung pathology that is suppressed by TCT (Figure 3I, J).

To further validate the transcriptomic predictions implicating NOD receptors, PGN release, and IL-1 cytokines as key modulators of *B. pertussis* induced inflammation, we assessed the IL-1β protein levels in the lung over the course of *B. pertussis* infection by ELISA. At 2-dpi, we observed significantly higher IL-1β levels in mice infected with the WT strain compared to those infected with TCT(+) (Figure 3M), indicating that TCT release suppresses IL-1β production and confirming predictions of our upstream regulator analysis (Figure 3I, J and M).

IL1 family cytokines reprogram airway fibroblasts, driving chemokine production and long-term lung remodeling following *B. pertussis* infection

To investigate how IL1 family cytokines contribute to inflammatory pathology and disease outcomes during *B. pertussis* infection, we used CellChat analysis to predict cytokine signaling networks using single cell RNA-sequencing data analysis of *B. pertussis* challenged mouse lungs. Neutrophils and AMs were identified as the dominant producers ('senders') of IL-1α and IL-1β transcriptis (Figure 4A, B). Unexpectedly, CellChat analysis predicted that airway fibroblasts 1 and 2 (AF1, AF2) were the primary receivers of IL-1α and IL-1β with few other populations showing appreciable expression of IL1 family receptor transcripts (Figure 4A, B). We also identified a putative signaling axis of IL-18-producing AMs signaling to IL18R+ basophils and NK cells (Figure 4B).

To investigate the response of airway fibroblasts to infection, we performed differential gene expression analysis on fibroblasts from infected versus PBS-sham challenged lungs, followed by Reactome pathway enrichment analysis (Figure 4C, D). Airway fibroblasts were found to express inflammation associated genes

e.g., *Cxcl10, Zbp1* and *Saa3,* and IFN-inducible genes e.g., *Gbp6* and *Stat1* (Figure 4C). Furthermore, this analysis revealed robust upregulation of Interleukin signaling pathway (Figure 4D). Additional enriched pathways included 'Extracellular matrix (ECM) reorganization' and 'Chemokine receptors bind chemokines' pathways (Figure 4D, E, F), suggesting that IL-1-activated airway fibroblasts may influence both the pronounced long-term pulmonary dysfunction and immune cell recruitment associated with *B. pertussis* infection (Figure 4D, E, F).

We hypothesized that IL1 family cytokine mediated activation of airway fibroblasts drives long-term collagen deposition and extracellular matrix reorganization following *B. pertussis* infection. Subsequently, we hypothesized that infection of mice with a TCT over-releasing strain (TCT(+)) would lead to reduced activation collagen deposition compared to challenge with WT *B. pertussis*. To test this, we performed long-term infection studies using WT, TCT(-) and TCT(+) *B. pertussis* strains. Lung tissue harvested at 6 months post-infection revealed significant collagen deposition in WT- and TCT(-)-infected mice, but markedly less in mice infected with the TCT(+) strain (Figure 4G). Differential gene expression analysis revealed significant upregulation of chemokines including Ccl7, Cxcl9, Cxcl5, Cxcl13, Cxcl10, Ccl19, and Cxcl16 in fibroblasts following infection (Figure 4F). These findings are consistent with our earlier bulk RNA-seq data: Cxcl13, Ccl19, and Cxcl5 were most highly expressed in TCT(-) infected lungs, while Cxcl19 and Cxcl10 were downregulated in TCT(+) infections compared to WT (Figure 1N, O), mapping the fibroblast chemokine signature to the TCT-dependent chemokine expression patterns observed in the bulk RNA sequencing.

We performed proteome profiling on lung lysates from WT, TCT(+) and TCT(-) infected mice to validate these transcriptomic predictions (Figure 4H). TCT(-) infection induced more IL-1α and IL-1β than WT or TCT(+) challenge (Figure 4I, J). Broadly, we observed higher chemokine levels in the TCT(-) group compared to the WT and TCT(+) infected mice (Figure 4I, J). Notably, protein levels of Cxcl13, Cxcl19, and Cxcl10 were highest in TCT(-) infected lungs and lowest in TCT(+) infected lungs (Figure 4I, J), mirroring gene expression trends and reinforcing the conclusion that airway fibroblasts are robust producers of chemokines and shape immune responses to *B. pertussis* following IL-1-mediated activation.

TCT limits adaptive immune cell recruitment and long-term immunity during *B. pertussis* infection by inhibiting NOD2 induced IL-1 family cytokine production

Several of the chemokines suppressed by TCT, have well-established roles in coordinating lymphocyte recruitment and priming adaptive immune responses. CXCL13 is essential for recruiting B cells to germinal centers and inflamed tissues, while CXCL9, CXCL10 and CCL19 mediate T cell recruitment to sites of inflammation[22-25]. Based on our transcriptomic data, we hypothesized that TCT-mediated suppression of these chemokines impairs adaptive immune cell infiltration into the lung and formation of germinal centers. To determine if TCT influences adaptive immune cell recruitment, we performed flow cytometry on 7-dpi lungs of mice infected with WT, TCT(-), or TCT(+) strains of *B. pertussis*. TCT release inversely correlated with recruitment of adaptive immune cells (Figure 5A-C). TCT(+) infected mice demonstrated decreased numbers of CD4, and CD8 T cells, and B cells in the lungs at 7-dpi compared WT infected mice, suggesting TCT release may be a mechanism to dampen recruitment of these cells (Figure 5A-C). Furthermore, TCT(-) infected mice, had significantly greater B cells in the lungs compared to WT infected mice, further implicating TCT in blocking recruitment and formation of adaptive immunity (Figure 5A-C).

To assess long-term immune consequences of TCT, we infected mice with WT, TCT(-) or TCT(+) *B. pertussis* strains and assessed lungs immunopathology at 6-months post-infection by H&E stain (Figure 5D). We observed formation and persistence of long-lived lymphoid structures in mice infected with *B. pertussis* compared to PBS challenged controls (Figure 5D). At 6 months post-infection, immune bronchus-associated lymphoid tissue (iBALT) structures were markedly reduced in the lungs of TCT(+) infected mice, suggesting that TCT suppresses the formation of long-lived lymphoid structures, limiting adaptive immune memory (Figure 5D, E).

As TCT is a NOD1 exclusive agonist, and our data suggests that NOD2 drives a stronger IL1-mediated induction of adaptive responses from airway fibroblasts than NOD1. We investigated the role of NOD1 and NOD2 in the formation of long-term immunity to *B. pertussis*. WT, NOD1, and NOD2 KO mice were infected with *B. pertussis* and lung-resident memory lymphocytes profiled at six months post-infection. Naïve B cell frequencies and germinal center B cell numbers were similar across groups (Figure 5F, G), but NOD1 KO mice exhibited significantly elevated lung resident memory B cells (IgD-CD38+GL7-) compared to WT mice (Figure 5G). Similarly, both central (CD44+CD62L+) and effector (CD44+CD62L-) memory CD4 T cells were increased

in NOD1 KO mice (Figure 5J, K), while naïve CD4+ T cell numbers remained unchanged (Figure 5H). These findings suggest that NOD1 signaling restricts adaptive memory formation, consistent with TCT's role as a NOD1-exclusive agonist. In NOD2 KO mice, we observed a modest increase in central memory CD4+ T cells, accompanied by an increase in naïve T cells, suggesting an expanded T cell pool rather than enhanced memory (Figure 5I, K).

To determine if IL-1 signaling is required for the immune cell recruitment and bacterial clearance, we challenged WT and IL1R1 KO mice with *B. pertussis* and evaluated inflammatory pathology, bacterial burden, and immune cell profiles. IL1R1 KO mice exhibited impaired bacterial clearance (Figure 5L), highlighting the essential role of IL-1 in pathogen control. Notably, despite higher bacterial burdens, IL1R1 KO mice exhibited significantly reduced pulmonary inflammation (Figure 5M), confirming IL-1's role as a central inflammatory mediator, and suggesting that differences in IL1 signaling may drive NOD2-dependent *B. pertussis* inflammation (Fig. 2E-G).

Surprisingly, innate immune cell recruitment (e.g., neutrophils, macrophages, and monocytes) was similar between WT and IL1R1 KO mice (Figure 5N-P). Yet strikingly, recruitment of both B and T cells was significantly diminished in IL1R1 KO mice compared to WT, indicating that IL-1 signaling, by recruited innate immune cells is crucial for adaptive immune cell infiltration into the lung (Figure 5R-T). Furthermore, a modest but significant decrease in dendritic cells was also observed in infected IL1R1 KO compared to WT controls, suggesting the bridging of the innate to adaptive response may be further hindered (Figure 5Q). Taken together, these findings support our hypothesis that TCT promotes *B. pertussis* immune evasion by skewing NOD1-driven responses to suppress a NOD2-mediated activation of AMs and release of IL-1 cytokines to drive the activation of IL1R1 expressing airway fibroblasts. Activation of these fibroblasts leads to enhanced chemokine expression, recruitment of adaptive immune cells and formation of germinal centers. This limits inflammation and compromises the development of protective immunity.

DISCUSSION

This study reveals a novel immune evasion strategy employed by *Bordetella pertussis*, selective release of a peptidoglycan fragment, TCT, which activates NOD1 while avoiding NOD2 engagement. This strategy parallels the way many Gram-negative bacteria modify their lipid A to modulate TLR4 engagement. We propose that *B. pertussis* has evolved a similar level of structural specificity in its PGN release to manipulate intracellular PRR signaling and evade immunity.

B. pertussis releases TCT during the turnover of saccular PGN is essential for bacterial growth and division. *B. pertussis* release of NOD1-activating TCT diminishes the release of NOD2 activating muropeptides. This strategy biases the host response toward NOD1 signaling, which we demonstrate results in less inflammation than activation of NOD2. This represents a previously unrecognized form of immune evasion based on selective release of structurally distinct cell wall fragments and highlights an unappreciated difference in disease outcomes following engagement of NOD1 or NOD2.

While both NOD1 and NOD2 signal through NF-kB, our data reveal distinct functional consequences *in vivo*[26]. NOD2 promotes pulmonary inflammation and facilitates bacterial clearance, but NOD1 suppresses inflammation and restrains the development of adaptive immunity. These data fit with recent in-silico work suggesting anhydrous peptidoglycan structures have anti-inflammatory roles, by blocking recognition of NOD2 and biasing towards NOD1[27]. These findings are supported by single-cell RNA-sequencing analyses demonstrating that NOD1 is broadly expressed across many cell types in the infected mouse lung, but NOD2 expression is restricted to inflammatory cells, including neutrophils, monocytes, alveolar macrophages and cDC2's. This restricted expression of NOD2 may contribute to its inflammatory potency. Additionally, NOD2's dual caspase recruitment (CARD) domains and its ability to engage mitochondrial antiviral signaling protein (MAVS) and type I IFN pathways, may further distinguish its activity from NOD1[28-30].

We identify a key downstream mechanism by which NOD2 signaling contributes to pulmonary pathology. Specifically, NOD2-driven IL1 production activates IL1R1+ airway fibroblasts, which in turn upregulate genes associated with extracellular matrix remodeling, collagen deposition and chemokine secretion. This fibroblast activation promotes immune cell infiltration and iBALT formation but also contributes to long-term tissue remodeling and fibrosis. In contrast, TCT limits IL1 production by avoiding NOD2 signaling, reducing fibroblast activation, chemokine secretion and immune infiltration. These findings connect PGN structural diversity to fibroblast activity and immune organization in the lung.

Interestingly, while IL1 was dispensable for neutrophil and monocyte recruitment, it was critical for B and CD4+ T cell infiltration and pathogen clearance. In IL1R1-deficient mice, we observed increased bacterial burden and impaired adaptive immunity, despite intact innate responses. Previous work by others in the field have linked IL-1β to bacterial clearance[31]. These results highlight the central role of the NOD2-IL1-fibroblast axis in orchestrating effective long-term immunity to *B. pertussis*. By skewing this axis, TCT promotes bacterial survival and immune evasion.

TCT release impaired the formation of iBALT and limited memory B and T cell development. These data suggest that early inhibition of IL1 production and fibroblast activation by TCT has long lasting consequences for adaptive immunity. Importantly, these findings explain how *B. pertussis* may evade long-term immune surveillance and establish persistent infection. Assessments of released PGN structures in previously and currently circulating clinical strains may provide further evidence of an evolutionary pressure on the availability and structure of muropeptides released by *pertussis*[32]. Further, these data have implications for other extracellular PGN producing infections such as *Neisseria gonorrhoeae* and *Borrelia burgdorferi*[9,33] for which the development of effective vaccines has been a persistent challenge.

These data also have direct implications for pertussis vaccine development. We suggest that selecting or engineering muropeptides that robustly stimulate NOD2 may improve immune priming, while vaccine strains lacking TCT could avoid the immunosuppressive effects we describe. Notably, the live attenuated *B. pertussis* vaccine candidate BPZE1 was engineered to lack TCT release[14,34]. Our data provide critical mechanistic support and biological justification for this approach, demonstrating that TCT release suppresses IL-1 production, restrains adaptive immune cell recruitment, and limits long-term immunity. Blocking TCT release, as in BPZE1, may therefore enhance immunogenicity and protection of future pertussis vaccines.

METHODS

Mice and ethics statement

All animal procedures were approved by the Institutional Animal Care and Use Committee at the University of Maryland School of Medicine (protocol 00000108). Adult (6–10-week-old) BALB/c and C57BL/6, NOD1 -/- NOD2 -/-, SLC46A2 -/-, and IL1R1 -/- mice were bred and housed under specific pathogen-free conditions.

Bacterial strains and infections

B. pertussis strains wild-type BC36, a streptomycin-resistant Tohama I derivative, isogenic mutants TCT(-), or TCT(+) were cultured on Bordet-Gengou agar supplemented with 10% defibrinated sheep blood or in Stainer-Scholte (SS) broth. Growth curves were generated by incubating strains of *B. pertussis* in 96-well plates, in 250 uL volume of SS broth, at starting ODs of 0.1, 0.05, and 0.01. Plate was incubated at 37C, shaking, and the OD was read every 10 minutes by the Cerillo Optical Density Microplate Reader. *B. pertussis* TCT mutant strains were generously supplied by William Goldman (University of North Carolina at Chapel Hill). TCT(+) strain was generated by expression of the *E. coli* AmpG in BC36, resulting in 24-fold increase in TCT release[15]. TCT(-) was generated by deletion of native *B. pertussis* AmpG and insertion of a kanamycin resistance gene at the site, resulting in a 50-fold decrease in TCT release[35]. Adult mice were anesthetized and inoculated intranasally with 2×10^6 CFU of *B. pertussis* in 50 µL PBS[36]. Lungs were harvested at 2, 4, 7, 14, 180 days post-infection for bacterial burden analysis by serial dilution and plating of homogenates, tissue sectioning and staining, RNA extraction, protein preparation, single cell preparation of lung-derived cells, and for flow cytometry analysis.

Histopathology and collagen staining

Lungs were fixed in 10% formalin, embedded in paraffin, and sectioned at 5 µm thickness. Slides were stained with hematoxylin and eosin (H&E) or mason's trichrome stain. Three blinded investigators scored sections for peribronchial and perivascular inflammation, alveolitis, and airway epithelial damage[37]. Bronchus associated lymphoid tissue (BALT) formation were tallied in the 180-dpi H&E stained lungs using ImageJ.

Flow cytometry analysis

Single cell suspensions were generated from the left lobe of mouse lungs using ACK lysis and collagenase digestion following the Cell STAR Protocols method for single-cell suspension preparation from murine organs, lung section[38]. After counting, cells were washed once with 1X PBS and stained for viability using Ghost Dye™ UV450 Viability dye (Tonbo Biosciences) diluted 1:1000 in 1X PBS for 10 minutes on ice. After viability staining, cells were washed once with 1X PBS containing BSA, sodium azide, and EDTA (FACS buffer). Fc receptors were blocked for in a solution containing 100µg/mL each of ChromPure™ mouse, rat, and hamster IgGs (Jackson ImmunoResearch Laboratories Inc.) in FACS buffer for 15 minutes on ice. Surface staining was performed next in FACS buffer for 15 minutes on ice. After surface staining, cells were washed twice with FACS buffer. Samples were analyzed on the Cytek Aurora 4, and all gating and compensation was generated using Flow Jo 10.8.1 (BD Biosciences).

RNA isolation and processing

Lung tissue was harvested at 2, 4, or 7-dpi for RNA isolation by the Trizol-choloroform method. Lung tissue was homogenized using the Omni Bead Beader (Omni, Inc), phase separated using chloroform and precipitated using isopropanol. RNA was then quantified and converted to cDNA (iScript cDNA Synthesis Kit). Quantitative real-time PCR (qPCR) was performed using the BIORAD CFX96 real-time PCR instrument. Gene expression was calculated as fold change relative to PBS-inoculated control animals using the $2^{-\Delta\Delta CT}$ threshold cycle method and normalized to Hypoxanthine phosphoribosyltransferase (HPRT) (internal housekeeping gene).

Bulk RNA sequencing

At 4-dpi, lungs were harvested from WT BALB/c mice (n = 3/group) infected with either WT, TCT(-), or TCT(+) strains of *B. pertussis*. Total RNA was extracted from homogenized lungs using Trizol Reagent (Invitrogen) according to the manufacturer's protocol. RNA integrity was confirmed using a Bioanalyzer (Agilent), and sequenced on an Illumina NextSeq 1000. FastQC and RSeQC were used to assess read and alignment quality. Reads were aligned with the *Mus musculus* GRCm39 reference genome. Differential gene expression was analyzed using DESeq2, with significance defined as adjusted p-value (FDR) < 0.05. QIAGEN proprietary Ingenuity pathway analysis (IPA) sub-package Upstream Regulator was performed on genes identified as differentially expressed between groups (WT vs TCT(-) and WT vs TCT(+)) and ranked by Z-activation score.

Single-Cell RNA sequencing

Single-cell suspensions were prepared from lung tissues of duplicate PBS-sham treated and Tohama-1 *B. pertussis* infected WT C57BL/6 mice at 4-dpi. Single cell preparation followed the published and validated Cell STAR Protocols method for single-cell suspension preparation from murine organs, lung section[38]. Following red blood cell lysis, cell viability was assessed by trypan blue staining, viable cells were enriched by (Miltenyi Biotec) Dead Cell Removal Kit and loaded onto the 10x Genomics Chromium Controller for barcoding and library construction. Sequencing was performed on an Illumina NovaSeq platform. Data were processed using Cell Ranger and analyzed using the Seurat v5 package in R. Quality control cutoffs of >1000 and <10,000 features and <20% mitochondrial RNA. Data were normalized via the standard Seurat workflow (NormalizeData, FindVariableFeatures, ScaleData) and individual Seurat processed samples were integrated via the Harmony method. LungMap Mouse CellCards Multi-Study CellRef 1.0 Atlas single cell dataset was utilized as a reference with known cell types to generate predictions for cell types in our single cell dataset. Clustering was performed via the Seurat package workflow (ScaleData, RunPCA, FindNeighbors, FindClusters, RunUMAP(dims = 1:30), RunTSNE(dims = 1:30). Clusters were annotated by the hallmark variable features determined by the software. DeSeq2 was performed to determine the differential gene expression between alveolar macrophages assessed as either NOD1 positive (0.25 expression level cutoff), NOD2 negative (0.25 expression level cutoff) and NOD2 positive, NOD1 negative. CellChat analysis performed on single cell dataset. Reactome pathway enrichment analysis performed on differential expressed genes identified (Wilcox) from PBS-sham and infection derived airway fibroblasts. Data visualized by Seurat (DimPlot, VInplot, DotPlot) and ggplot2 (Volcano, HeatMap) R packages.

Lung protein preparation and quantification

At 2, 4 and 7-dpi, lungs were harvested from WT BALB/c mice (n = 5/group) infected with either WT, TCT(-), or TCT(+) strains of *B. pertussis*. Lungs were homogenized in PBS with protease inhibitors and treated with Triton X-100 (1%). Samples were freeze-thawed at -80C and then centrifuged to remove cellular debris. 7DPI lung samples (n = 5) were pooled for each group (PBS, WT, TCT(-), and TCT(+)) and processed by bio-techne Proteome Profiler Array, Mouse Cytokine Array Panel A (Catalog # ARY006) protocol. Resulting array was quantified by ImageJ analysis. 2, 4, and 7-dpi lung samples (n = 5) were assessed by bio-techne Mouse IL-1 beta/IL-1F2 ELISA Kit (Catalog # MLB00C) protocol.

Reporter cell assays for NOD1 and NOD2 activation

HEK293-derived reporter cells expressing murine or human NOD1 and NOD2 with an NF-kB inducible SEAP reporter (InvivoGen) were stimulated with *B. pertussis* tracheal cytotoxin, TCT (generously provided by William Goldman, UNC), live *B. pertussis* strains (MOI of 400), and the conditioned media from the bacteria grown in Stainer-Scholte (SS) media. *B. pertussis* strains were grown to log phase, and the spent media was collected at OD 0.8. Spent media was centrifuged and filtered to remove bacteria and large fragments. Supernatants were analyzed for reporter activity using colorimetric detection kits (InvivoGen).

FIGURE LEGENDS

Figure 1. Representative 40x stitched H&E stains of *B. pertussis* strains (**A**) WT, (**B**) TCT(-), and (**C**) TCT(+) 7-dpi BALB/c mouse lungs and **(D)** inflammatory histology scores for mice intranasally challenged with $2x10^6$ CFU. (**E**) Bacterial burden in the lungs at 2, 7, and 14-dpi. Number of (**F**) CD45+CD11b+Ly6g+ (Neutrophils), (**G**) CD45+CD11b+CD14+ (Macrophages), (**H**) CD45+Ly6cHI ClassII+ (Inflammatory Monocytes), and (**I**) CD45+CD11c+CD14- (Dendritic cells), and the percent of (**J**) CD45+CD206+ (M2-skewed) and (**K**) CD45+CD86+ (M1-skewed) cells in the 7-dpi lungs of BALB/c mice challenged with WT, TCT(-), or TCT(+) strains of *B. pertussis*. Bulk transcriptomic volcano plots comparing 4-dpi lungs of BALB/c mice infected with (**L**) WT vs TCT(-) or (**M**) WT vs TCT(+). Heat map of bulk transcriptomic comparisons, highlighting cytokines and chemokines which were differentially regulated between (**N**) WT vs TCT(-) or (**O**) WT vs TCT(+).

Figure 2. Murine NOD1 response to either (**A**) live *B. pertussis* (MOI 400) or (**B**) *B. pertussis* conditioned media (5%) and measured by HEK293 reporter cells with an NF-kB based SEAP reporter, assessed at 655nm. Murine NOD1 response to either (**C**) live *B. pertussis* (MOI 400) or (**D**) *B. pertussis* conditioned media (5%) and measured by HEK293 reporter cells with an NF-kB based SEAP reporter, assessed at 655nm. H&E stains of C57/B6 mice intranasally challenged with $2x10^6$ CFU for (**E**) WT, (**F**) NOD1 KO and (**G**) NOD2 KO 7-dpi lungs, (**H**) bacterial burden in the lungs at 2, 4, and 7-dpi, (**I**) inflammatory lung histology scores at 7-dpi. Number of (**J**) CD45+CD11b+Ly6g+ (Neutrophils), (**K**) CD45+CD11b+CD14+ (Macrophages), (**L**) CD45+Ly6cHI ClassII+ (Inflammatory Monocytes), and (**M**) CD45+CD11c+CD14- (Dendritic cells), and the percent of (**N**) CD45+C11b+CD14+CD86+ (M1-skewed macrophage) and (**O**) CD45+CD11b+CD14+CD206+ (M2-skewed macrophage) cells in the 4-dpi lungs of C57/B6 WT, NOD1 KO, and NOD2 KO mice challenged with WT parental strain of *B. pertussis*. *il1b* transcript levels in 2-dpi lungs of WT, NOD1 KO, NOD2 KO mice challenged with WT strain of *B. pertussis*.

Figure 3: UMAP of (**A**) predicted cell types and (**B**) sample derived ID from single cell sequencing of PBS-sham challenged and *B. pertussis* infected C57/B6 mouse lungs at 4-dpi. (**C**) Comparison of relative abundance of cell types across infected and uninfected sample IDs. Cell type specific expression of (**D**) *nod1* and (**E**) *nod2* in the 4-dpi *B. pertussis* challenged mouse lung. (**F**) UMAP of subclustered alveolar macrophages (AM), (**G**) identified cluster markers, and (**H**) cluster specific expression for *nod1*, *nod2*, *il1b*, and *il1a* from the single cell *B. pertussis* challenged mouse lung dataset. Upstream regulator analysis via the Ingenuity pathway analysis (IPA) pipeline comparing the 4-dpi lungs of BALB/c mice infected with (**I**) WT vs TCT(-) or (**J**) WT vs TCT(+), measured by Z-activation score for the relative upstream regulators annotated in the pipeline. (**K**) Single cell analysis of 4-dpi alveolar macrophages assessed for NOD1 and NOD2 expression greater than 0.25 relative expression, grouping cells into NOD1+NOD2+, NOD1+NOD2-, NOD1-NOD2+, and NOD1-NOD2-. (**L**) Differential gene expression analysis comparing NOD1+NOD2- cells vs NOD1-NOD2+ cells derived from the 4-dpi single cell dataset. (**M**) IL-1B lung protein levels assessed by ELISA for WT, TCT(-), and TCT(+) infected BALB/c mice at 2, 4, and 7-dpi.

Figure 4. (**A** and **B**) CellChat analysis performed on single cell sequencing of PBS-sham challenged and *B. pertussis* infected C57/B6 mouse lungs at 4-dpi, identifying cell types predicted as involved in IL1 signaling. (**C**) Differential gene expression analysis performed on airway fibroblasts derived from infected (4-dpi) or uninfected mice then (**D**) Reactome pathway enrichment analysis performed, implicating (**E**) extracellular matrix reorganization and (**F**) chemokine pathways. (**G**) Representative 10x images of mason's trichrome stain of 180-dpi lungs from mice challenged with WT, TCT(-), and TCT(+) strains of *B. pertussis*. (**H**) Proteome profiler array of pooled 7-dpi and PBS-sham lung lysates from WT, TCT(-), and TCT(+) challenged mice, quantified via ImageJ analysis (**I** and **J**).

Figure 5. Number of (**A**) CD45+CD4+CD8- (CD4 T cells), (**B**) CD45+CD4-CD8+ (CD8 T cells), and (**C**) CD45+CD19+ClassII+ (B cells) in 7-dpi lungs of BALB/c mice challenged with *B. pertussis*. (**D**) Representative 4 and 10x images of H&E stains of PBS sham and *B. pertussis* strains WT, TCT(-), and TCT(+) 180-dpi BALB/c mouse lungs and **(E)** number of bronchi associated lymphoid tissue (BALT) in each 180-dpi lung sample. Number of (**F**) CD19+IgD+CD38+ (Naïve B cells), (**G**) CD19+IgD-CD38-GL7+ (Germinal Center B cells), (**H**) CD19+IgD-CD38+GL7- (Memory B cells), (**I**) TCRβ+CD4+CD44-CD62L+ (Naïve CD4 T cells), (**J**) TCRβ+CD4+CD44+CD62L- (Effector Memory CD4 T cells), (**K**) TCRβ+CD4+CD44+CD62L+ (Central Memory CD4 T cells) cells in 180-dpi lungs from C57/B6 WT, NOD1 KO, and NOD2 KO mice challenged with WT Tohama-1 derived parental strain of *B. pertussis*. (**L**) Bacterial load and (**M**) inflammatory histology score of H&E stained 7-dpi lungs from C57/B6 WT and IL1R1 KO mice intranasally challenged with $2x10^6$ CFU. Number of (**N**) CD45+CD11b+Ly6g+ (Neutrophils), (**O**) CD45+CD11b+CD14+ (Macrophages), (**P**) CD45+Ly6cHI ClassII+ (Inflammatory Monocytes), and (**Q**) CD45+CD11c+CD14- (Dendritic cells), (**R**) CD45+CD19+ClassII+ (B cells), (**S**) CD45+CD4+CD8- (CD4 T cells), and (**T**) CD45+CD4-CD8+ (CD8 T cells) cells in the 7-dpi lungs of C57/B6 WT and IL1R1 KO mice challenged with WT strain of *B. pertussis*.

Supplemental Figure 1. (**A**) Doubling time assessed by analysis of (**B**) growth curve of WT, TCT(-), and TCT(+) strains grown in SS broth. Number of (**C**) CD45+CD11b+Ly6g+ (Neutrophils), (**D**) CD45+CD11b+CD14+ (Macrophages), (**E**) CD45+Ly6cHI ClassII+ (Inflammatory Monocytes), and (**F**) CD45+CD11c+CD14- (Dendritic cells), in the 4-dpi lungs of BALB/c mice challenged with WT, TCT(-), or TCT(+) strains of *B. pertussis*.

Supplemental Figure 2. (**A**) Murine or (**B**) human NOD1 response to purified TCT and C12-iE-DAP control, and (**C**) Murine or (**D**) human NOD2 response to purified TCT and L18-MDP control, measured by HEK293 reporter cells with an NF-kB based SEAP reporter, assessed at 655nm.

Supplemental Figure 3. (**A**) Feature UMAP and cell type specific (**B**) violin plot for SLC46A2, mapping expression of the transcript in the single cell C57/B6 4-dpi lungs. (**C**) Bacterial burden and (**D**) inflammatory scoring of H&E stained 7-dpi WT C57/B6 and SLC46A2 KO mice infected with WT parental, TCT(-), and TCT(+) strains of *B. pertussis*.

Supplemental Figure 4. KEGG pathway analysis of differentially expressed genes for alveolar macrophage clusters (**A**) 1 and (**B**) 2 compared to other subclusters of alveolar macrophages in the *B. pertussis* challenged single cell 4-dpi C57/B6 murine lungs. GO pathway enrichment analysis of (**C**) NOD2 and (**D**) NOD1 associated genes in alveolar macrophages from the single cell 4-dpi C57/B6 murine lungs.

Figure 1.

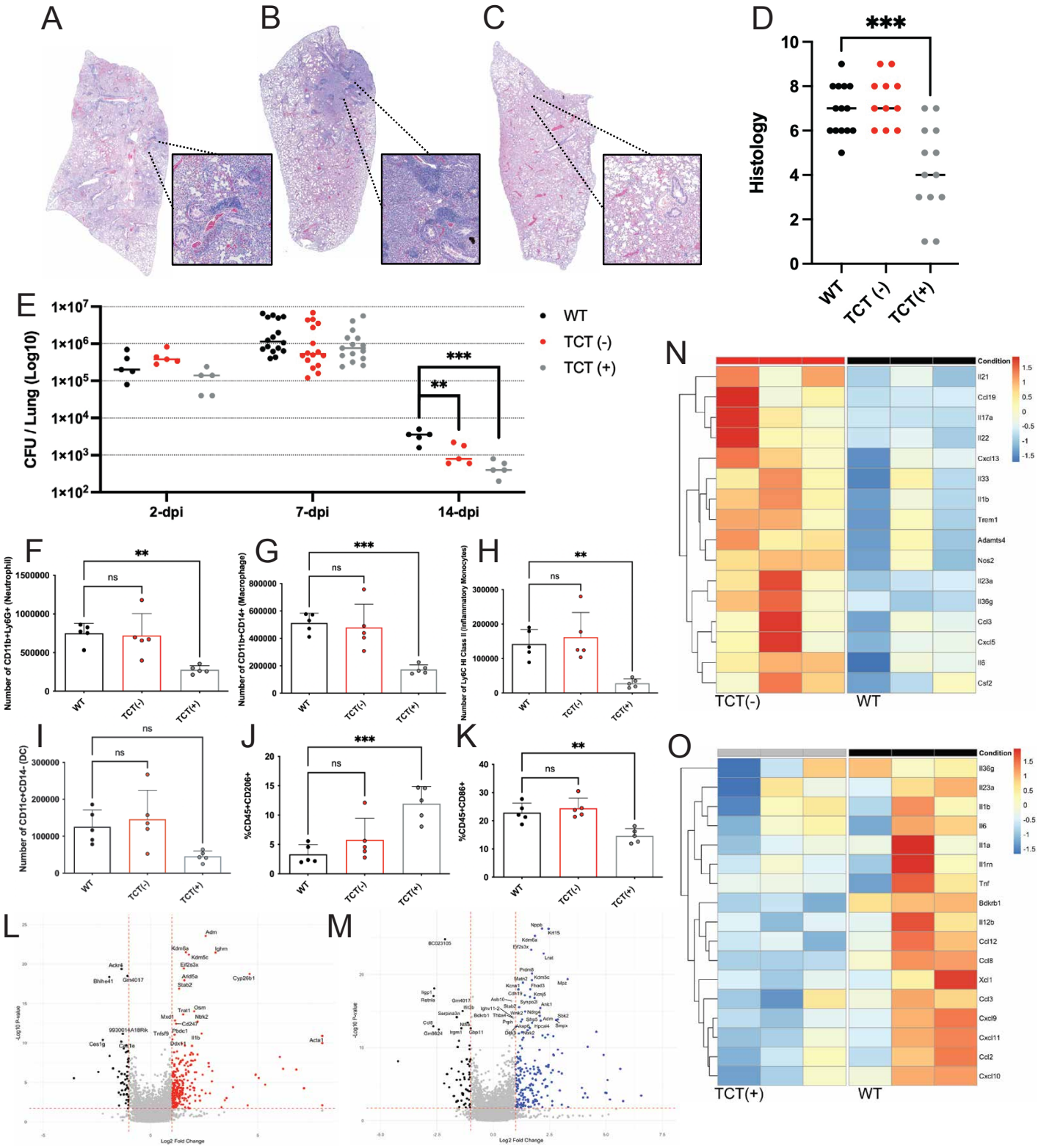
A
B
C
D
***
Histology
WT
TCT (-)
TCT(+)
E
CFU / Lung (Log10)
1×10^7
1×10^6
1×10^5
1×10^4
1×10^3
1×10^2
WT
TCT (-)
TCT (+)
***
**
2-dpi
7-dpi
14-dpi
F
Number of CD11b+Ly6G+ (Neutrophil)
G
Number of CD11b+CD14+ (Macrophage)
H
Number of Ly6C Hi Class II (Inflammatory Monocytes)
I
Number of CD11c+CD14- (DC)
J
%CD45+CD206+
K
%CD45+CD86+
ns
N
Condition
Il21
Ccl19
Il17a
Il22
Cxcl13
Il33
Il1b
Trem1
Adamts4
Nos2
Il23a
Il36g
Ccl3
Cxcl5
Il6
Csf2
TCT(-)
WT
O
Condition
Il36g
Il23a
Il1b
Il6
Il1a
Il1rn
Tnf
Bdkrb1
Il12b
Ccl12
Ccl8
Xcl1
Ccl3
Cxcl9
Cxcl11
Ccl2
Cxcl10
TCT(+)
WT
L
M
Log2 Fold Change
-Log10 P-value

Figure 2.

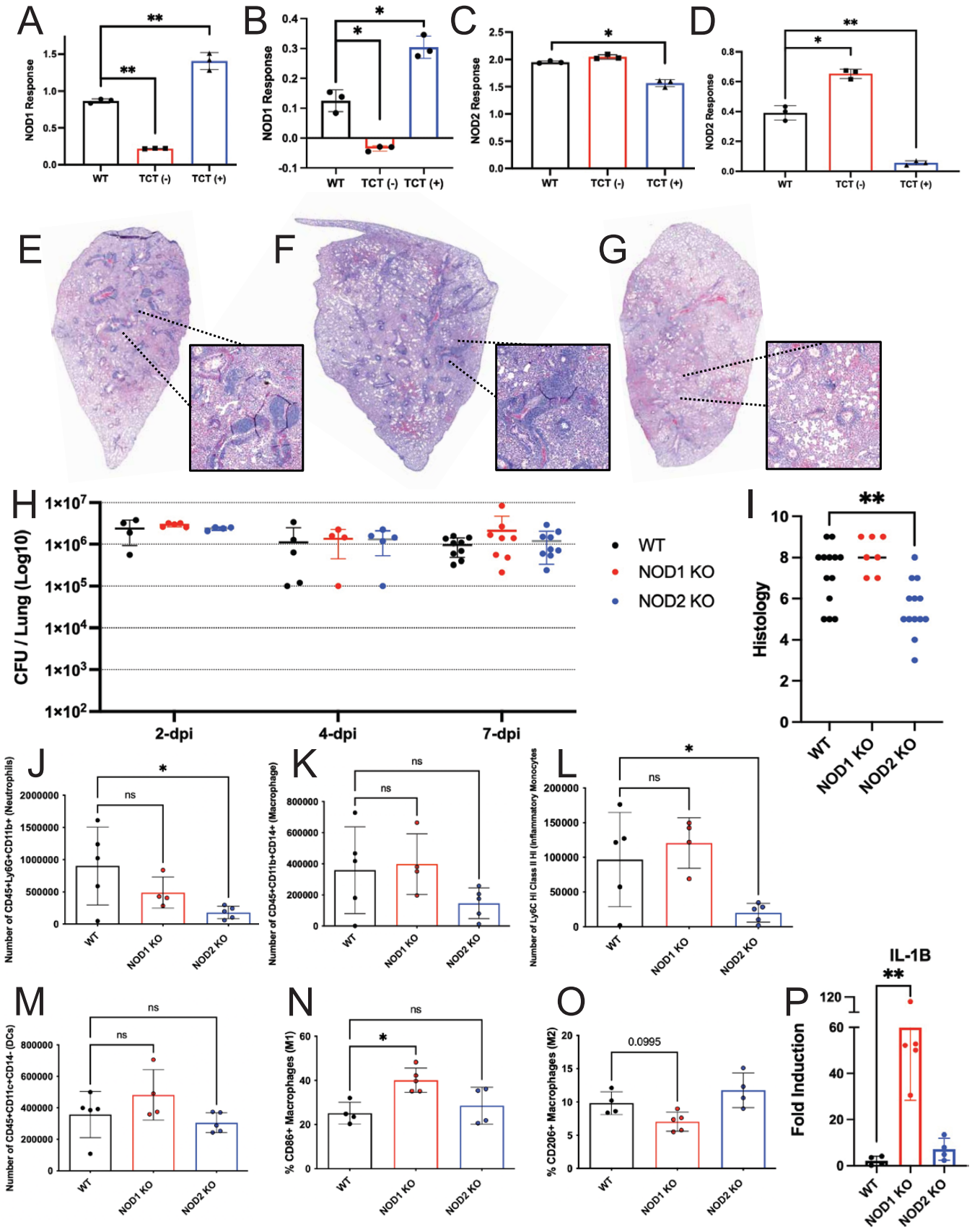
A
NOD1 Response
WT
TCT (-)
TCT (+)
B
NOD1 Response
C
NOD2 Response
D
NOD2 Response
E
F
G
H
CFU / Lung (Log10)
2-dpi
4-dpi
7-dpi
WT
NOD1 KO
NOD2 KO
I
Histology
J
Number of CD45+Ly6G+CD11b+ (Neutrophils)
K
Number of CD45+CD11b+CD14+ (Macrophage)
L
Number of Ly6C Hi Class II Hi (Inflammatory Monocytes
M
Number of CD45+CD11c+CD14- (DCs)
N
% CD86+ Macrophages (M1)
O
% CD206+ Macrophages (M2)
0.0995
P
IL-1B
Fold Induction
ns

Figure 3.

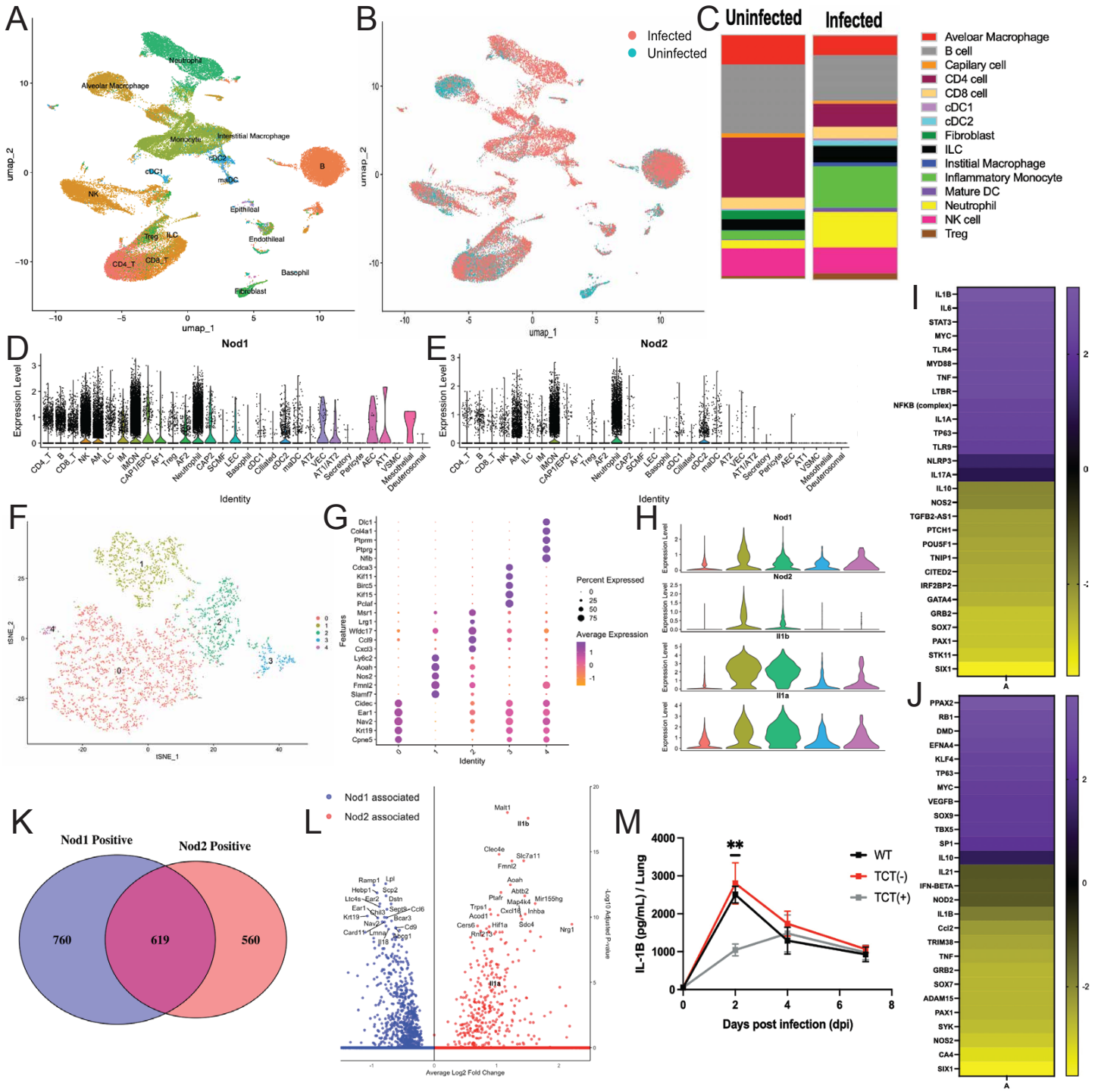
A
B
C
Uninfected
Infected
Infected
Uninfected
Aveolar Macrophage
B cell
Capilary cell
CD4 cell
CD8 cell
cDC1
cDC2
Fibroblast
ILC
Institial Macrophage
Inflammatory Monocyte
Mature DC
Neutrophil
NK cell
Treg
umap_1
umap_2
D
Nod1
E
Nod2
Expression Level
Identity
F
G
H
I
J
K
Nod1 Positive
Nod2 Positive
760
619
560
L
Nod1 associated
Nod2 associated
Average Log2 Fold Change
-Log10 Adjusted P-value
M
IL-1B (pg/mL) / Lung
Days post infection (dpi)
WT
TCT(-)
TCT(+)
**

Figure 4.

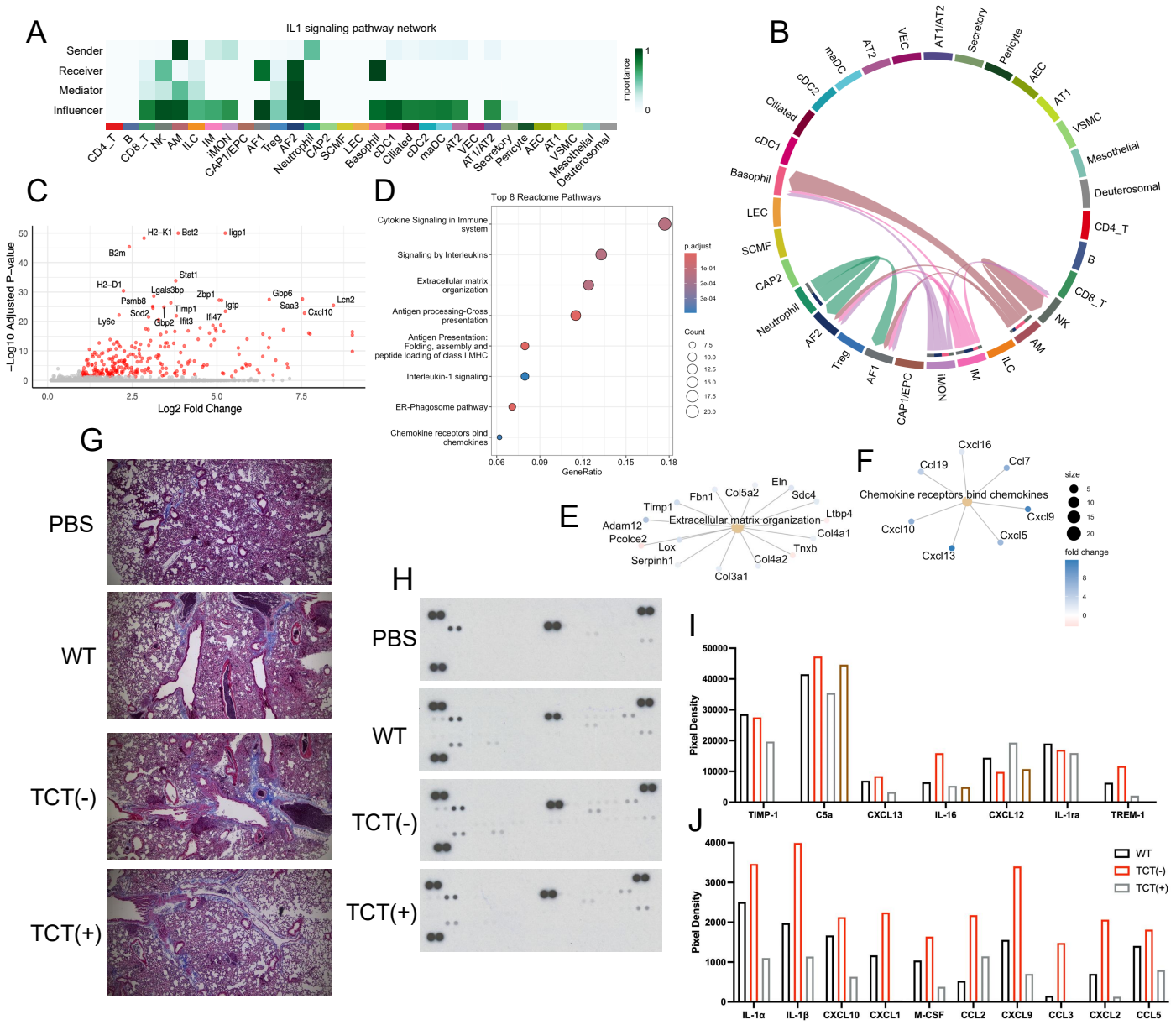
A
IL1 signaling pathway network
Sender
Receiver
Mediator
Influencer
Importance
CD4_T
B
CD8_T
NK
AM
ILC
IM
IMON
CAP1/EPC
AF1
Treg
AF2
Neutrophil
CAP2
SCMF
LEC
Basophil
cDC1
Ciliated
cDC2
maDC
AT2
VEC
AT1/AT2
Secretory
Pericyte
AEC
AT1
VSMC
Mesothelial
Deuterosomal
B
C
−Log10 Adjusted P−value
Log2 Fold Change
H2−K1
Bst2
Iigp1
B2m
Stat1
H2−D1
Lgals3bp
Zbp1
Gbp6
Psmb8
Igtp
Saa3
Lcn2
Sod2
Timp1
Cxcl10
Ly6e
Gbp2
Ifit3
Ifi47
D
Top 8 Reactome Pathways
Cytokine Signaling in Immune system
Signaling by Interleukins
Extracellular matrix organization
Antigen processing-Cross presentation
Antigen Presentation: Folding, assembly and peptide loading of class I MHC
Interleukin-1 signaling
ER-Phagosome pathway
Chemokine receptors bind chemokines
GeneRatio
p.adjust
Count
E
Extracellular matrix organization
Fbn1
Col5a2
Eln
Sdc4
Timp1
Ltbp4
Adam12
Col4a1
Pcolce2
Lox
Tnxb
Serpinh1
Col4a2
Col3a1
F
Chemokine receptors bind chemokines
Cxcl16
Ccl19
Ccl7
Cxcl9
Cxcl10
Cxcl5
Cxcl13
size
fold change
G
PBS
WT
TCT(-)
TCT(+)
H
PBS
WT
TCT(-)
TCT(+)
I
Pixel Density
TIMP-1
C5a
CXCL13
IL-16
CXCL12
IL-1ra
TREM-1
J
Pixel Density
WT
TCT(-)
TCT(+)
IL-1α
IL-1β
CXCL10
CXCL1
M-CSF
CCL2
CXCL9
CCL3
CXCL2
CCL5

Figure 5.

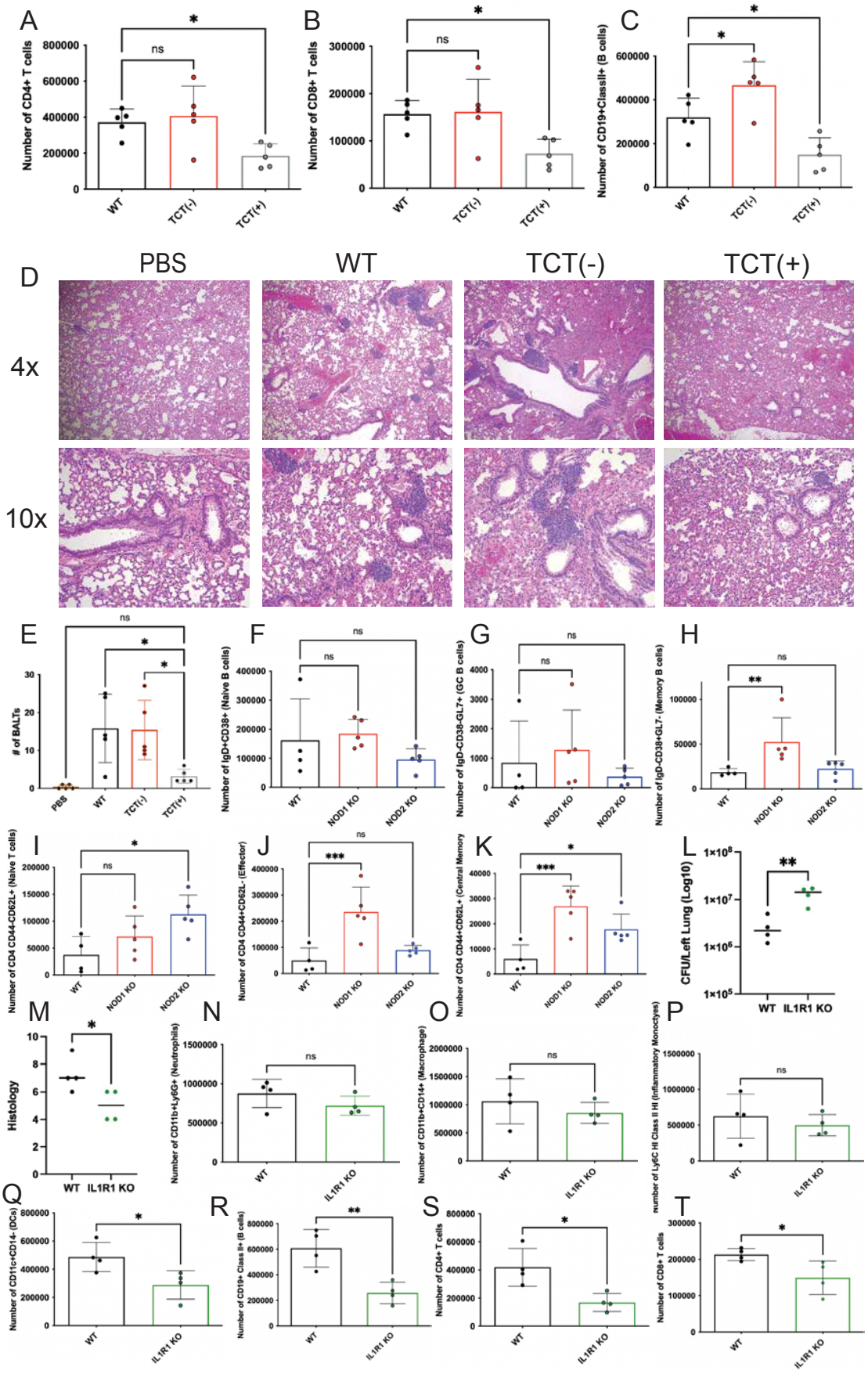
A
Number of CD4+ T cells
WT
TCT(-)
TCT(+)
B
Number of CD8+ T cells
C
Number of CD19+ClassII+ (B cells)
D
PBS
WT
TCT(-)
TCT(+)
4x
10x
E
# of BALTs
F
Number of IgD+CD38+ (Naive B cells)
NOD1 KO
NOD2 KO
G
Number of IgD-CD38-GL7+ (GC B cells)
H
Number of IgD-CD38+GL7- (Memory B cells)
I
Number of CD4 CD44-CD62L+ (Naive T cells)
J
Number of CD4 CD44+CD62L- (Effector)
K
Number of CD4 CD44+CD62L+ (Central Memory
L
CFU/Left Lung (Log10)
IL1R1 KO
M
Histology
N
Number of CD11b+Ly6G+ (Neutrophils)
O
Number of CD11b+CD14+ (Macrophage)
P
number of Ly6C Hi Class II Hi (Inflammatory Monoctyes)
Q
Number of CD11c+CD14- (DCs)
R
Number of CD19+ Class II+ (B cells)
S
Number of CD4+ T cells
T
Number of CD8+ T cells

References

1. Needham, B.D., and Trent, M.S. (2013). Fortifying the barrier: the impact of lipid A remodelling on bacterial pathogenesis. Nat Rev Microbiol *11*, 467–481. 10.1038/nrmicro3047.
2. Garde, S., Chodisetti, P.K., and Reddy, M. (2021). Peptidoglycan: Structure, Synthesis, and Regulation. EcoSal Plus *9*. doi:10.1128/ecosalplus.ESP-0010-2020.
3. Chamaillard, M., Hashimoto, M., Horie, Y., Masumoto, J., Qiu, S., Saab, L., Ogura, Y., Kawasaki, A., Fukase, K., Kusumoto, S., et al. (2003). An essential role for NOD1 in host recognition of bacterial peptidoglycan containing diaminopimelic acid. Nat Immunol *4*, 702–707. 10.1038/ni945.
4. Girardin, S.E., Boneca, I.G., Viala, J., Chamaillard, M., Labigne, A., Thomas, G., Philpott, D.J., and Sansonetti, P.J. (2003). Nod2 is a general sensor of peptidoglycan through muramyl dipeptide (MDP) detection. J Biol Chem *278*, 8869–8872. 10.1074/jbc.C200651200.
5. Stafford, C.A., Gassauer, A.-M., de Oliveira Mann, C.C., Tanzer, M.C., Fessler, E., Wefers, B., Nagl, D., Kuut, G., Sulek, K., Vasilopoulou, C., et al. (2022). Phosphorylation of muramyl peptides by NAGK is required for NOD2 activation. Nature *609*, 590–596. 10.1038/s41586-022-05125-x.
6. Rosenthal, R.S., Nogami, W., Cookson, B.T., Goldman, W.E., and Folkening, W.J. (1987). Major fragment of soluble peptidoglycan released from growing Bordetella pertussis is tracheal cytotoxin. Infect Immun *55*, 2117–2120. 10.1128/iai.55.9.2117-2120.1987.
7. Woodhams, K.L., Chan, J.M., Lenz, J.D., Hackett, K.T., and Dillard, J.P. (2013). Peptidoglycan fragment release from Neisseria meningitidis. Infect Immun *81*, 3490–3498. 10.1128/iai.00279-13.
8. Goldman, W.E., and Cookson, B.T. (1988). Structure and functions of the Bordetella tracheal cytotoxin. Tokai J Exp Clin Med *13 Suppl*, 187–191.
9. Chan, J.M., and Dillard, J.P. (2016). Neisseria gonorrhoeae Crippled Its Peptidoglycan Fragment Permease To Facilitate Toxic Peptidoglycan Monomer Release. J Bacteriol *198*, 3029–3040. 10.1128/jb.00437-16.
10. Luker, K.E., Collier, J.L., Kolodziej, E.W., Marshall, G.R., and Goldman, W.E. (1993). Bordetella pertussis tracheal cytotoxin and other muramyl peptides: distinct structure-activity relationships for respiratory epithelial cytopathology. Proc Natl Acad Sci U S A *90*, 2365–2369. 10.1073/pnas.90.6.2365.
11. Kessie, D.K., Lodes, N., Oberwinkler, H., Goldman, W.E., Walles, T., Steinke, M., and Gross, R. (2020). Activity of Tracheal Cytotoxin of Bordetella pertussis in a Human Tracheobronchial 3D Tissue Model. Front Cell Infect Microbiol *10*, 614994. 10.3389/fcimb.2020.614994.
12. Jacobs, C., Huang, L.J., Bartowsky, E., Normark, S., and Park, J.T. (1994). Bacterial cell wall recycling provides cytosolic muropeptides as effectors for beta-lactamase induction. Embo j *13*, 4684–4694. 10.1002/j.1460-2075.1994.tb06792.x.
13. Adin, D.M., Engle, J.T., Goldman, W.E., McFall-Ngai, M.J., and Stabb, E.V. (2009). Mutations in ampG and lytic transglycosylase genes affect the net release of peptidoglycan monomers from Vibrio fischeri. J Bacteriol *191*, 2012–2022. 10.1128/jb.01547-08.
14. Mielcarek, N., Debrie, A.-S., Raze, D., Bertout, J., Rouanet, C., Younes, A.B., Creusy, C., Engle, J., Goldman, W.E., and Locht, C. (2006). Live Attenuated B. pertussis as a Single-Dose Nasal Vaccine against Whooping Cough. PLOS Pathogens *2*, e65. 10.1371/journal.ppat.0020065.
15. RS, L. (2001). Tracheal cytotoxin production by the Bordetellae. PhD thesis. Washington University, St. Louis, MO.
16. Mantovani, A., Sica, A., and Locati, M. (2005). Macrophage polarization comes of age. Immunity *23*, 344–346. 10.1016/j.immuni.2005.10.001.

17. Paik, D., Monahan, A., Caffrey, D.R., Elling, R., Goldman, W.E., and Silverman, N. (2017). SLC46 Family Transporters Facilitate Cytosolic Innate Immune Recognition of Monomeric Peptidoglycans. J Immunol *199*, 263–270. 10.4049/jimmunol.1600409.
18. Magalhaes, J.G., Philpott, D.J., Nahori, M.A., Jéhanno, M., Fritz, J., Le Bourhis, L., Viala, J., Hugot, J.P., Giovannini, M., Bertin, J., et al. (2005). Murine Nod1 but not its human orthologue mediates innate immune detection of tracheal cytotoxin. EMBO Rep *6*, 1201–1207. 10.1038/sj.embor.7400552.
19. Le Bourhis, L., Benko, S., and Girardin, S.E. (2007). Nod1 and Nod2 in innate immunity and human inflammatory disorders. Biochem Soc Trans *35*, 1479–1484. 10.1042/bst0351479.
20. Kimura, Y., Kimura, M., Miura, N., Yoshino, Y., and Kono, H. (2025). NOD1 deficiency promotes inflammation via autophagic degradation of ASK1. Commun Biol *8*, 781. 10.1038/s42003-025-08213-6.
21. Bharadwaj, R., Lusi, C.F., Mashayekh, S., Nagar, A., Subbarao, M., Kane, G.I., Wodzanowski, K.A., Brown, A.R., Okuda, K., Monahan, A., et al. (2023). Methotrexate suppresses psoriatic skin inflammation by inhibiting muropeptide transporter SLC46A2 activity. Immunity *56*, 998–1012.e1018. 10.1016/j.immuni.2023.04.001.
22. Gunn, M.D., Ngo, V.N., Ansel, K.M., Ekland, E.H., Cyster, J.G., and Williams, L.T. (1998). A B-cell-homing chemokine made in lymphoid follicles activates Burkitt's lymphoma receptor-1. Nature *391*, 799–803. 10.1038/35876.
23. Tannenbaum, C.S., Tubbs, R., Armstrong, D., Finke, J.H., Bukowski, R.M., and Hamilton, T.A. (1998). The CXC chemokines IP-10 and Mig are necessary for IL-12-mediated regression of the mouse RENCA tumor. J Immunol *161*, 927–932.
24. Zhang, Y., Liu, G., Zeng, Q., Wu, W., Lei, K., Zhang, C., Tang, M., Zhang, Y., Xiang, X., Tan, L., et al. (2024). CCL19-producing fibroblasts promote tertiary lymphoid structure formation enhancing anti-tumor IgG response in colorectal cancer liver metastasis. Cancer Cell *42*, 1370–1385.e1379. 10.1016/j.ccell.2024.07.006.
25. Kersh, A.E., Sati, S., Huang, J., Murphy, C., Ahart, O., and Leung, T.H. (2024). CXCL9, CXCL10, and CCL19 synergistically recruit T lymphocytes to skin in lichen planus. JCI Insight *9*. 10.1172/jci.insight.179899.
26. Heim, V.J., Stafford, C.A., and Nachbur, U. (2019). NOD Signaling and Cell Death. Front Cell Dev Biol *7*, 208. 10.3389/fcell.2019.00208.
27. Kwan, J.M.C., Liang, Y., Ng, E.W.L., Sviriaeva, E., Li, C., Zhao, Y., Zhang, X.L., Liu, X.W., Wong, S.H., and Qiao, Y. (2024). In silico MS/MS prediction for peptidoglycan profiling uncovers novel anti-inflammatory peptidoglycan fragments of the gut microbiota. Chem Sci *15*, 1846–1859. 10.1039/d3sc05819k.
28. Kanneganti, T.D., Lamkanfi, M., and Núñez, G. (2007). Intracellular NOD-like receptors in host defense and disease. Immunity *27*, 549–559. 10.1016/j.immuni.2007.10.002.
29. Sabbah, A., Chang, T.H., Harnack, R., Frohlich, V., Tominaga, K., Dube, P.H., Xiang, Y., and Bose, S. (2009). Activation of innate immune antiviral responses by Nod2. Nat Immunol *10*, 1073–1080. 10.1038/ni.1782.
30. Domínguez-Martínez, D.A., Pérez-Flores, M.S., Núñez-Avellaneda, D., Torres-Flores, J.M., León-Avila, G., García-Pérez, B.E., and Salazar, M.I. (2024). NOD2 Responds to Dengue Virus Type 2 Infection in Macrophage-like Cells Interacting with MAVS Adaptor and Affecting IFN-α Production and Virus Titers. Pathogens *13*. 10.3390/pathogens13040306.
31. Place, D.E., Muse, S.J., Kirimanjeswara, G.S., and Harvill, E.T. (2014). Caspase-1-independent interleukin-1β is required for clearance of Bordetella pertussis infections and whole-cell vaccine-mediated immunity. PLoS One *9*, e107188. 10.1371/journal.pone.0107188.
32. Hovingh, E.S., van Gent, M., Hamstra, H.J., Demkes, M., Mooi, F.R., and Pinelli, E. (2017). Emerging Bordetella pertussis Strains Induce Enhanced Signaling of Human Pattern

Recognition Receptors TLR2, NOD2 and Secretion of IL-10 by Dendritic Cells. PLoS One *12*, e0170027. 10.1371/journal.pone.0170027.
33. Jutras, B.L., Lochhead, R.B., Kloos, Z.A., Biboy, J., Strle, K., Booth, C.J., Govers, S.K., Gray, J., Schumann, P., Vollmer, W., et al. (2019). Borrelia burgdorferi peptidoglycan is a persistent antigen in patients with Lyme arthritis. Proceedings of the National Academy of Sciences *116*, 13498–13507. doi:10.1073/pnas.1904170116.
34. Keech, C., Miller, V.E., Rizzardi, B., Hoyle, C., Pryor, M.J., Ferrand, J., Solovay, K., Thalen, M., Noviello, S., Goldstein, P., et al. (2023). Immunogenicity and safety of BPZE1, an intranasal live attenuated pertussis vaccine, versus tetanus-diphtheria-acellular pertussis vaccine: a randomised, double-blind, phase 2b trial. Lancet *401*, 843–855. 10.1016/s0140-6736(22)02644-7.
35. Skerry, C.M., Cassidy, J.P., English, K., Feunou-Feunou, P., Locht, C., and Mahon, B.P. (2009). A live attenuated Bordetella pertussis candidate vaccine does not cause disseminating infection in gamma interferon receptor knockout mice. Clin Vaccine Immunol *16*, 1344–1351. 10.1128/cvi.00082-09.
36. Skerry, C., Goldman, W.E., and Carbonetti, N.H. (2019). Peptidoglycan Recognition Protein 4 Suppresses Early Inflammatory Responses to Bordetella pertussis and Contributes to Sphingosine-1-Phosphate Receptor Agonist-Mediated Disease Attenuation. Infect Immun *87*. 10.1128/IAI.00601-18.
37. Gallop, D., Scanlon, K.M., Ardanuy, J., Sigalov, A.B., Carbonetti, N.H., and Skerry, C. (2021). Triggering Receptor Expressed on Myeloid Cells-1 (TREM-1) Contributes to Bordetella pertussis Inflammatory Pathology. Infect Immun *89*, e0012621. 10.1128/IAI.00126-21.
38. Ndeupen, S., Qin, Z., and Igyártó, B.Z. (2022). Single-cell suspension preparation from murine organs following in vivo mRNA-LNP exposure. STAR Protocols *3*, 101350. https://doi.org/10.1016/j.xpro.2022.101350.